Journal of the European Ceramic Society **15** (1995) 173–184

0955-2219/95/$9.50

Reaction Process and Densification Process of Mixed α'/β'-Sialon Ceramics

Koji Watari, Masaki Yasuoka, Maria Cecilia Valecillos & Shuzo Kanzaki

Department of Ceramics Science, National Industrial Research Institute of Nagoya, Hirate-cho, Kita-ku, Nagoya, 462 Japan

(Received 3 May 1994; revised version received 24 June 1994; accepted 5 July 1994)

Abstract

The sintering behavior of mixed α'/β'-sialon ceramics, fabricated from α-Si_3N_4, AlN and Ln_2O_3 (Y_2O_3, Er_2O_3 and Yb_2O_3), was examined by high-temperature dilatometry, and the densification process was discussed through the consideration of chemical reactions to form α'- and β'-sialon and kinetical analysis of shrinkage. The formation of α'-sialon and melilite caused temporary retardation of the densification rate, while during the formation of β'-sialon the densification proceeded remarkably. The densification accompanied by precipitation of β'-sialon is ascribed to dissolution of residual α-Si_3N_4, α'-sialon with low solid solubility and melilite into a liquid, which may result in an increase of liquid volume and in a decrease of liquid viscosity. These phenomena are considered to induce the solution–precipitation process, particle disintegration process and cooperative flow process of the particle–liquid mixture, yielding to rapid shrinkage. The densification at the initial and middle stages and the reactions from α'-sialon and α-Si_3N_4 to β'-sialon accelerated in the order of Y_2O_3 > Er_2O_3 > Yb_2O_3 addition, because the liquidus temperature and viscosity of liquid formed decreased in the order of Y_2O_3 < Er_2O_3 < Yb_2O_3 addition.

1 Introduction

Two significant properties of silicon nitride (Si_3N_4) ceramics are mechanical strength and fracture toughness. Si_3N_4 ceramics with prismatic grains show high flexural strength at room temperature, but this strength degrades at temperatures higher than 1300°C due to the presence of an intergranular glassy phase containing impurities such as metals and halogens. As the viscosity of the glassy phase softens at temperatures higher than 1000°C, grain-boundary sliding occurs, accompanied by nucleation and growth of cavities in the intergranular glassy phase.[1] It is then important to reduce the amount of impurities concentrated at the grain boundaries, and to control the character and amount of grain-boundary phase in Si_3N_4 ceramics, in order to improve their high-temperature strength.

On the other hand, fracture toughness is strongly influenced by aspect ratio and volume fraction of the grown grains in the final products.[2,3] It has been reported that Si_3N_4 ceramics with microstructures consisting of elongated rod-like grains in the small grain matrix have fracture toughness as high as 8–11 $MPam^{0.5}$.[4] Such materials with duplex microstructures are called 'in-situ composites' or 'self-reinforced materials'. It is, therefore, desirable for the obtention of the Si_3N_4-based materials that both the reduction of glassy phase content at grain boundaries and the control of Si_3N_4 grain morphology are made compatible.

Si_3N_4 ceramics occur in two structural modifications, α and β. The solid solution in β-Si_3N_4, which is called β'-sialon, is formed by simultaneous equivalent substitution of aluminum and oxygen for silicon and nitrogen, and the reaction is commonly described by the following equations:

$$(4 - z)Si_3N_4 + 2zAlN + zSiO_2 \rightarrow 2Si_{6-z}Al_zO_zN_{8-z} \quad (1)$$

$$(6 - z)Si_3N_4 + zAlN + zAl_2O_3 \rightarrow 3Si_{6-z}Al_zO_zN_{8-z} \quad (2)$$

In the equations, z takes a value between 0 and 4·2.[5,6]

α'-sialon, which is the solid solution of α-phase structure, is obtained by a substitution of similar elements as for β'-sialon, with some metal cations accommodated in the two large interstices of the unit cell, thus giving a general formula of the type $Mx(Si,Al)_{12}(O,N)_{16}$, where M is Li, Mg, Ca or

lanthanide metals except La and Ce. When x is $0{\cdot}3 < x < 2{\cdot}0$, single-phase α'-sialons are fabricated. Reaction in the formation of single-phase α'-sialon is as follows:[7,8]

$$(4 - 1{\cdot}5x)Si_3N_4 + 0{\cdot}5x(Y_2O_3 + 9AlN) \rightarrow Yx Si_{12-4{\cdot}5x}Al_{4{\cdot}5x}O_{1{\cdot}5x}N_{16-1{\cdot}5x} \quad (3)$$

With x values less than 0·3, mixtures of α'-sialon and β'-sialon are obtained.[9]

Densification of these sialon ceramics proceeds in a reaction-sintering process involving the formation of a transient liquid phase, namely, during the middle and final stages of sintering the ingredients of the liquid are incorporated into the α and β structures.[9–11] In consequence, sialon ceramics have been expected to possess only a small amount of intergranular glassy phase and in recent years these materials have been reported to maintain the room-temperature strength at temperatures as high as 1300°C.[12] It has been, however, reported by several investigators that single-phase sialon ceramics show lower mechanical strength and lower fracture toughness than β-Si_3N_4 containing Y_2O_3 and Al_2O_3 additives. The reason is interpreted as that sialons consist of grains with low aspect ratio,[13] and furthermore they have weak pullout and absence of crack-branching effects due to the strong bonding between interfaces of grains.[14,15]

Recently, mixed α'/β'-sialon ceramics have received a great deal of attention, since the microstructure of these materials comprises prismatic β-grains and roundish fine α-grains, and presents a small amount of grain boundary phase.[16,17] It has also been demonstrated that they show higher mechanical strength at elevated temperatures and higher fracture toughness[16] as well as better creep properties, compared to the β-Si_3N_4 ceramics with oxide addition.[18] Furthermore, in the case of sintering of mixed α'/β'-sialon ceramics, their microstructure and their mechanical as well as thermal properties can be controlled by the phase composition, and it is possible to alter widely the quantity and type of elements that can be accommodated in a Si_3N_4 structure.[15,19] However, the densification mechanism, which links directly to control of the microstructural development and phase composition, has not been understood yet.

In this work, an attempt is made to investigate the reaction process in the formation of α'- and β'-sialons during sintering of mixed α'/β'-sialon ceramics with AlN and lanthanide oxides (Ln_2O_3) such as Y_2O_3, Er_2O_3 and Yb_2O_3. The shrinkage behavior of mixed α'/β'-sialon ceramics is studied by high-temperature dilatometry, and the densification process is also discussed in combination with chemical reactions to form sialons.

2 Experimental procedure

It is well known that powder characteristics strongly influence the sintering process of sialon as well as of Si_3N_4 ceramics. Especially, in the case of sintering of mixed α'/β'-sialon ceramics, accompanied by complicated reaction pathways, densification behavior and resultant amount of α'-sialon, as well as reaction sequence, are changed due to powder characteristics.[20] In a preliminary work, the authors have evaluated the influence of Si_3N_4 powder characteristics on the sintering behavior of mixed α'/β,-sialon ceramics, and on the sinterability and formation of α'- and β'-sialons. The results pertaining to sintering behavior are as indicated in the Appendix, and the raw powder A was used in this work. The raw powder A (Denki Kagaku Kogyo, K K, Japan) used in the present work had an oxygen content of 1·3wt%, total metallic impurities content of 350 ppm, fluorine content of 520 ppm, and a specific surface area of 11·3 $m^2\ g^{-1}$. This powder was composed of 94% α- and 6% β-Si_3N_4.

The AlN (Tokuyama Soda Co. Ltd, Japan), Y_2O_3, Er_2O_3 and Yb_2O_3 (Hokko Chemicals Industry Co. Ltd, Japan) powders were also employed as the starting materials to produce the mixed α'/β'-sialon. The starting AlN powder had an oxygen content of 1·05 wt% and a specific surface area of 3·2 $m^2\ g^{-1}$. Nominal composition of powder mixtures was 83·10 mol% for Si_3N_4, 1·69 mol% for AlN and 15·21 mol% for Ln_2O_3, and the atomic proportion in the overall composition is represented by the following formula: $Ln_{0{\cdot}15}Si_{11{\cdot}325}Al_{0{\cdot}675}O_{0{\cdot}225}N_{15{\cdot}775}$.

These powders were vibrationally mixed in toluene with deflocculant for 6 h using a Si_3N_4 pot and balls. After drying at 800°C for 1 h in nitrogen gas with 10% H_2 to remove the deflocculant, rectangular bars with dimensions of 10 × 10 × 45 mm and discs with 14 mm diameter × 8 mm height were made from the mixed powders using a homemade die, followed by cold isostatic pressing (CIP) at 490MPa for 60s. The green density of all the specimens was 1950 ± 20 kgm^{-3}.

In order to investigate the sintering phenomena, thermal shrinkage of bars was measured at temperatures from 1000 to 1850°C at a heating rate of 10°C min^{-1} under a N_2 gas pressure of 1 MPa using a high-temperature dilatometer (Rigaku Denki, HPHT-TMA, Japan).[21] From the results of preliminary work, a large amount of shrinkage was observed after thermal shrinkage measurement at 1850°C, when operated at a heating rate of 10°C min^{-1}. Therefore, the heating rate of 10°C min^{-1} was selected. Isothermal shrinkage measurements at 1500, 1550 and 1600°C were performed

to investigate the kinetic parameter on densification and to clarify the densification process. The heating rate for isothermal shrinkage measurements was 10°C min^{-1}. The reason for setting such a slow heating rate will be explained later. Detection errors of shrinkage and shrinkage rate were less than $1{\cdot}8 \times 10^{-2}$% and $3{\cdot}2 \times 10^{-3}$ %min^{-1}, respectively.

Simultaneously, specimens were prepared by firing at various temperatures followed by quenching, to observe the change in bulk density and microstructural development as well as the reaction sequence during sintering. The discs were embedded in a mixture of Si_3N_4/AlN/Ln_2O_3/BN in a graphite crucible, and fired in a graphite furnace at different temperatures starting from 1300 to 1850°C for 15 min and 4 h at a heating rate of 10°C min^{-1} under a N_2 gas pressure of 1 MPa, followed by quenching at a cooling rate of above 100°C min^{-1} until near 1000°C.

Density measurements were performed by the Archimedes method in distilled water. Relative density was obtained by comparing measured density to theoretical density. The theoretical density of mixed α'/β'-sialon was calculated from the amount and density of Si_3N_4, AlN and Ln_2O_3, and was estimated as 3221 kgm^{-3} for Y_2O_3 addition, 3288 kgm^{-3} for Er_2O_3 addition, and 3296 kgm^{-3} for Yb_2O_3 addition. Carbon and gold were evaporated onto the fractured surfaces and onto the polished surfaces, and scanning electron microscopy (SEM, JEOL, T-330AS, Japan) observation was conducted to examine the microstructure. Before the evaporation of carbon and gold, the surfaces of interest were chemically etched by immersing the specimens into molten NaOH and KOH in a silver crucible at 200°C.

The quenched samples were crushed in a tungsten carbide jar, and passed through a 200 mesh sieve. X-ray diffractometry (XRD, Rigaku Denki, RAD-B, Japan) measurements of the crushed powders were carried out using CuK_α radiation at 40kV and 100 mA to identify crystalline phase and to obtain phase composition. The α-Si_3N_4, α'-sialon, and β-Si_3N_4/β'-sialon contents in the sintered bodies were determined as follows: after XRD measurements, the X-ray peak areas of α-Si_3N_4 and α'-sialon for <102> and <201> planes, and of β-Si_3N_4/β'-sialon for <101> and <201> planes were calculated using the Lorents function, and the relative amount of these phases was obtained by comparing their peak areas. Lattice parameters were measured with Si as internal standard, and the solid solubility of AIN and oxide into a Si_3N_4 structure was determined by referring to the published data.[22,23]

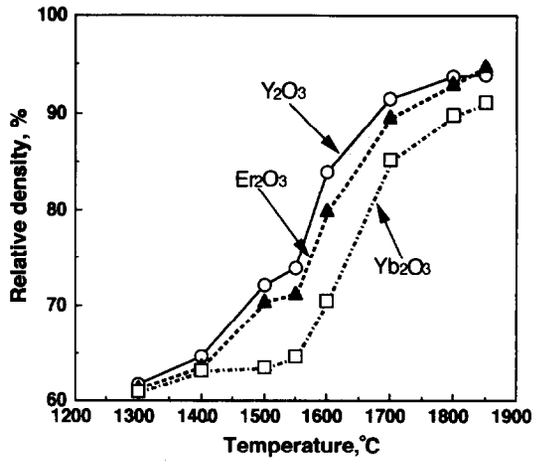

Fig. 1. Relative density of disks quenched at different temperatures for 15 min. The theoretical density of mixed α'/β'-sialon was calculated from the amount and density of Si_3N_4, AlN and Ln_2O_3, and was estimated as 3221 kgm^{-3} for Y_2O_3 addition, 3288 kgm^{-3} for Er_2O_3 addition and 3296 kgm^{-3} for Yb_2O_3 addition. After sintering at 1850°C for 4 h, bulk density of all the specimens reached theoretical values.

3 Results

3.1 Density and shrinkage

The relative densities of the discs quenched from different temperatures in the range of 1300 to 1850°C are shown in Fig. 1. For Y_2O_3 and Er_2O_3 additions, relative density increases slowly at temperatures between 1300 and 1550°C, and increases rapidly at temperatures between 1550 and 1800°C. On the other hand, the relative density of specimens obtained by Yb_2O_3 addition remains almost constant at temperatures from 1300 to 1550°C, whereas a rapid increase in the relative density was observed at temperatures higher than 1550°C. After sintering at 1850°C for 4 h, bulk density of all the specimens reached the theoretical values.

Figure 2 shows the shrinkage of rectangular bars. The shrinkage of all the compacts starts

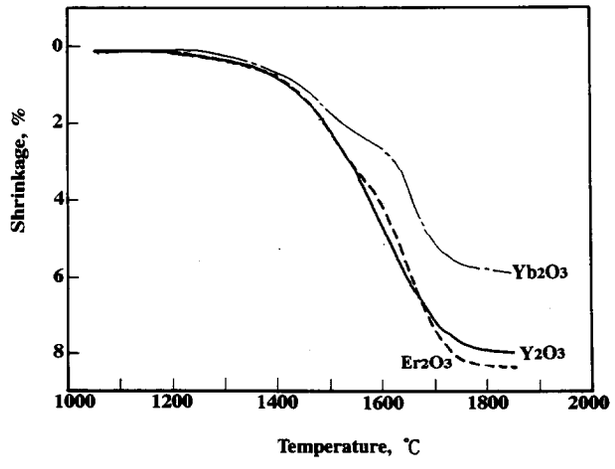

Fig. 2. Temperature dependence of shrinkage of Ln_2O_3-doped α'/β'-sialon ceramics.

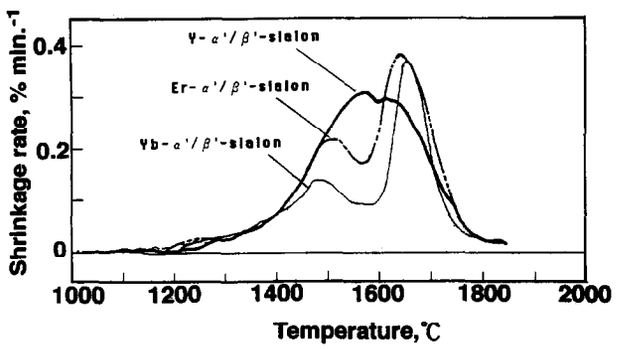

Fig. 3. Temperature dependence of shrinkage rate of Ln_2O_3-doped α'/β'-sialon.

around 1200°C, and increases with increasing the sintering temperature. The type of lanthanide oxides produces differential sintering behavior, which translates into the changes of shrinkage rate observed in the curves of Fig. 3. In the case of Y_2O_3 addition, the shrinkage rate increases gradually at temperatures higher than 1350°C, and reaches the maximum around 1570°C. Subsequently, the shrinkage rate shows a slight decrease and again an increase at temperatures between 1570 and 1620°C, decreasing rapidly at temperatures higher than 1620°C. For Er_2O_3 and Yb_2O_3 additions, the shrinkage rate shows an increase up to 1510°C for Er_2O_3 addition, and 1480°C for Yb_2O_3 addition, decreasing thereafter until reaching the vicinity of 1580°C. At temperatures over 1580°C, the shrinkage rate presents a rapid increase, showing a maximum at 1630°C for Er_2O_3 addition, and at 1650°C for Yb_2O_3 addition, decreasing thereafter with increasing sintering temperature.

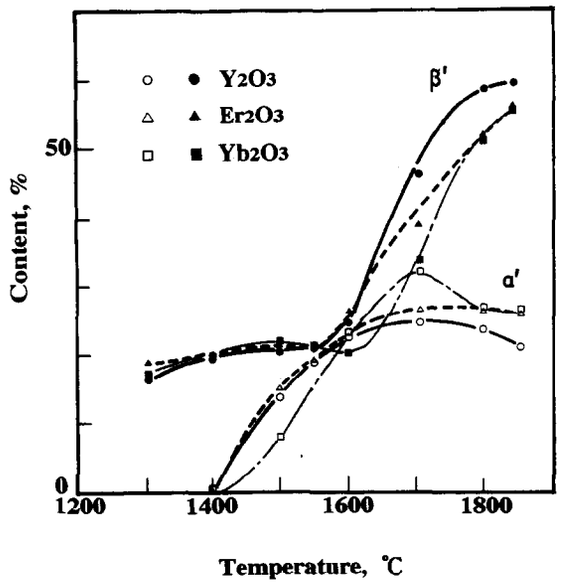

Fig. 4. Phase change during the formation of α'/β'-sialon ceramics at temperatures between 1300 and 1850°C. *J*-phase ($Ln_4Si_2O_7N_2$) and melilite ($Si_3N_4{\cdot}Ln_2O_3$) were identified as the grain boundary phase in specimens sintered at 1300–1400°C and at 1500–1700°C, respectively.

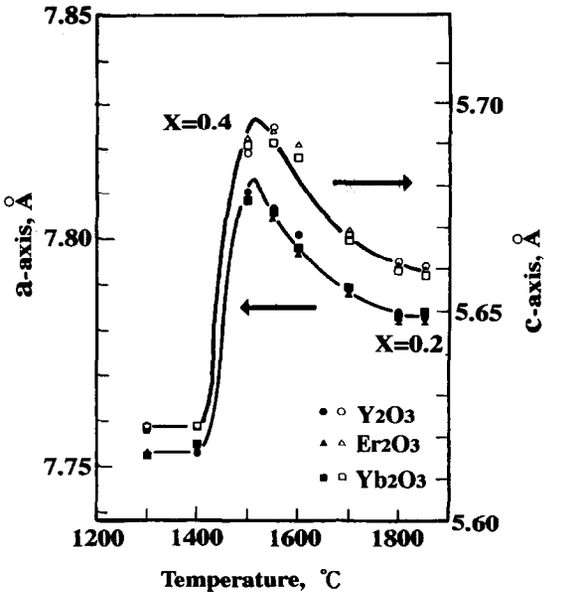

Fig. 5. Change of lattice parameters of α'-sialon. From the relationships between the x value in $Yx(Si,Al)_{12}(O,N)_{16}$ and lattice parameters,[21] the x value was 0·4 for the specimen heated at 1500°C and 0·25 for the specimen heated at 1850°C.

3.2 Phase change

Figure 4 reveals the phase change during the formation of α'- and β'-sialons at temperatures between 1300 and 1850°C. Also the variation with temperature of the lattice parameters of α'- and β'-sialons are shown in Figs 5 and 6, respectively.

α-sialon with large unit cell dimensions is initially formed at temperatures between 1400 and 1500°C, and its content increases with raising the sintering temperatures, but decreases above 1700°C . The amount of α'-sialon varies with the

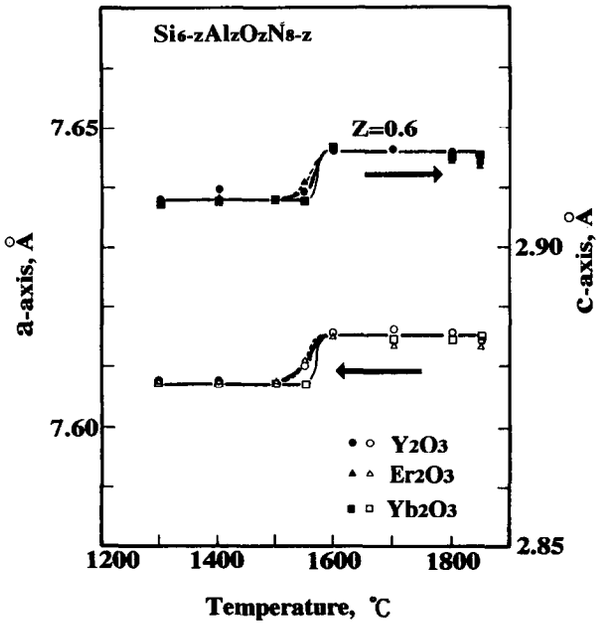

Fig. 6. Change of lattice parameters of β'-sialon. Referring to the relationships between the z value and lattice parameters,[22] the value of z in the formula, $Si_{6-z}Al_zO_zN_{8z}$, varies from 0 to 0·6 at temperatures from 1500 to 1600°C.

type of oxides. A rapid increase in the amount of α'-sialon is observed at temperatures between 1400 and 1600°C for Y_2O_3 and Er_2O_3 additions, and at temperatures between 1500 and 1700°C for Yb_2O_3 addition. Lattice parameters of α'-sialon attain a maximum at 1530°C, but thereafter decrease as the temperature is raised. The influence of the type of lanthanide oxide on the lattice parameters has not been identified in the present work. From the relationships between the x value in $Yx(Si, Al)_{12}$ $(O, N)_{16}$ and the lattice parameters,[22] the x value is 0·4 for the specimen obtained at 1500°C and 0·25 for the one at 1850°C.

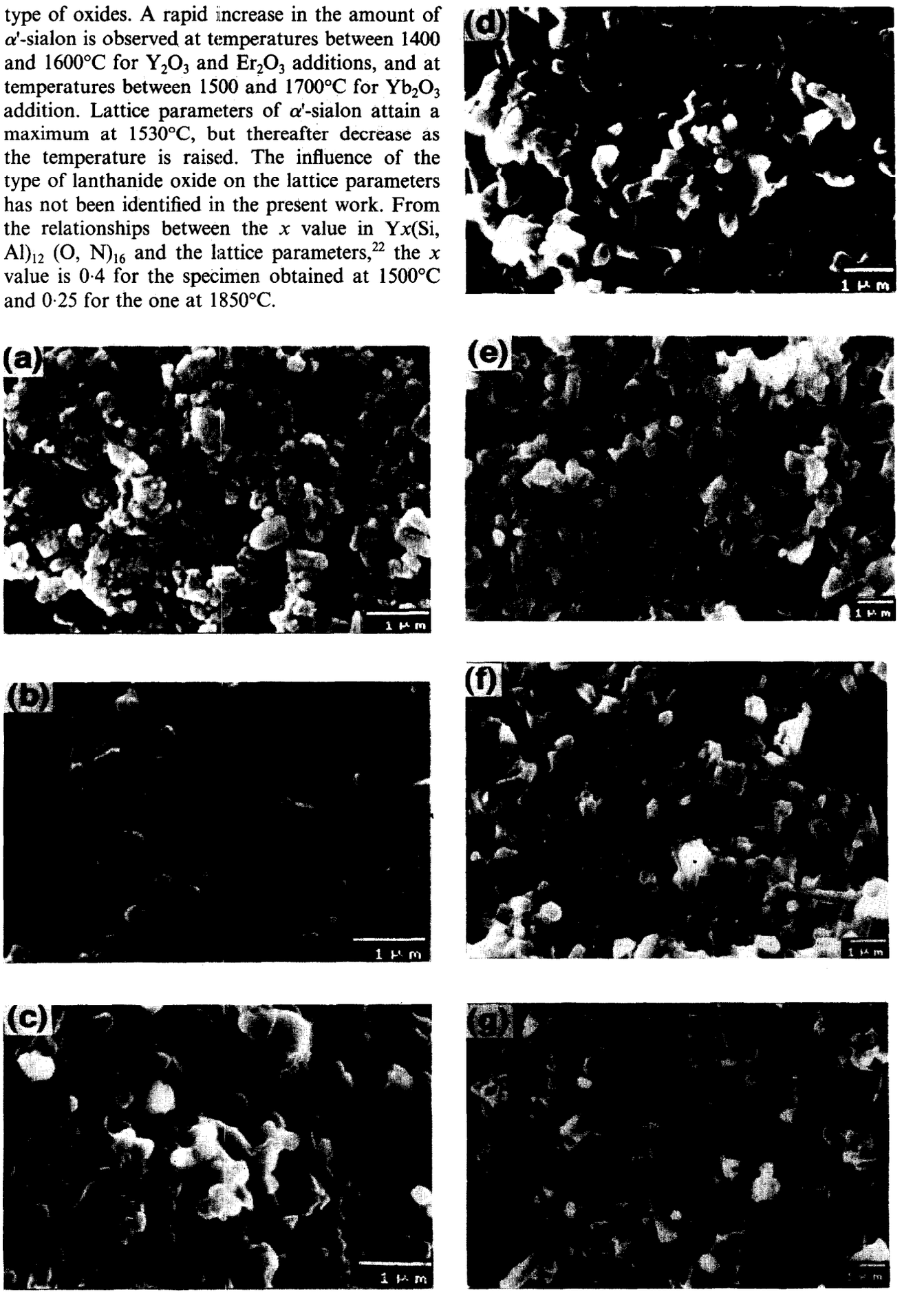

Fig. 7. Fractured surface and polished surface of a specimen with Er_2O_3 addition (a) CIPed, and quenched at (b) 1400, (c) 1500, (d) 1600, (e) 1700, (f) 1800 and (g) 1850°C for 15 min and (h) at 1850°C for 4 h. The polished surface of the specimen quenched at 1850°C for 4 h was chemically etched with molten NaOH and KOH at 200°C for 15 min.

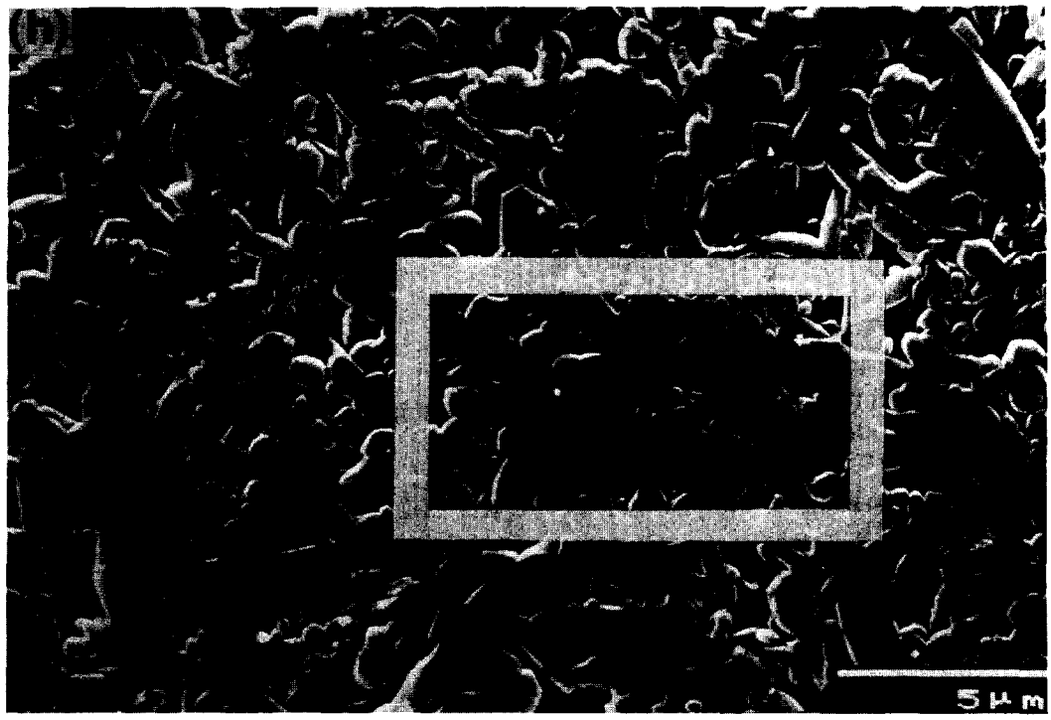

Fig. 7.—*Contd.*

A remarkable increase in the amount of β'-sialon is observed at temperatures ranging from 1600 to 1700°C for Y_2O_3 and Er_2O_3 additions, and at temperatures ranging from 1600 to 1800°C for Yb_2O_3 addition. A significant change in the lattice parameters is present at temperatures between 1500 and 1600°C, but the influence of the oxide type on lattice parameters is not detected. According to published data,[23] the value of z in the formula, $Si_{6-z}Al_zO_zN_{8-z}$, was 0·6 for the specimen sintered at temperatures higher than 1600°C.

Identification of X-ray diffraction peaks indicates, besides the formation of α'- and β'-sialons, J-phase ($Ln_4Si_2O_7N_2$) and melilite (Si_3N_4 . Ln_2O_3) in specimens quenched at temperatures between 1300 and 1400°C, and at temperatures between 1500 and 1700°C, respectively. Disappearance of X-ray diffraction peaks of raw AlN and Ln_2O_3 was recognized above 1500 and 1300°C, respectively.

3.3 Microstructure

Fractured surface of specimens with Er_2O_3 addition CIPed and sintered at temperatures between 1400 and 1850°C are shown in Fig. 7. The microstructure of CIPed specimens consists of grains with irregular shape and wide particle distribution (Fig. 7(a)). At temperatures from 1400 to 1600°C, the size and shape of particles are not well defined (Fig. 7 (b)–(d)), because the particles are covered with a material like a glassy phase. Elongated angular grains are found in specimens quenched from 1700°C (Fig. 7 (e) and (f)), and subsequent grain growth and interlocking are observed at 1850°C (Fig. 7 (g)). The microstructure of the specimens sintered at 1850°C for 4 h consists of rod-like grains with aspect ratio of around 5 : 1 and a maximum of about 8 : 1 in a small equiaxed grains matrix (Fig. 7(h)).

Figure 8 shows the fractured surface of specimens with Y_2O_3 and Yb_2O_3 addition obtained by quenching from 1400°C. In the case of Yb_2O_3 addition, roundish grains are found, but in the case of Y_2O_3 addition, identification of size and shape of particles in the fractured surface is difficult.

Table 1. Possible reactions to form the α'- and β'-sialons[a]

α'-Sialon

$SiO_2 + Al_2O_3 + Ln_2O_3 + Si_3N_4/AlN \rightarrow$ Nitrogen glass + J-Phase ($Ln_4Si_2O_7N_2$) (a)

J-Phase + Nitrogen glass + Si_3N_4/AlN $\rightarrow$ α'-Sialon^H + Melilite(Si_3N_4 . Ln_2O_3) + Nitrogen glass (b)

$Si_3N_4 + 9AlN$. $Ln_2O_3 \rightarrow \alpha'$-Sialon^H (c)

$Si_3N_4 + \alpha'$-Sialon$^H \rightarrow \alpha'$-Sialon^L (d)

β'-Sialon

Si_3N_4 + Melilite + Nitrogen glass $\rightarrow$ β'-Sialon + Nitrogen glass (e)

$Si_3N_4 + \alpha'$-Sialon^L + Nitrogen glass $\rightarrow$ β'-Sialon + Nitrogen glass (f)

[a] H and L indicate the α'-sialons with high and low solid solubility, respectively.

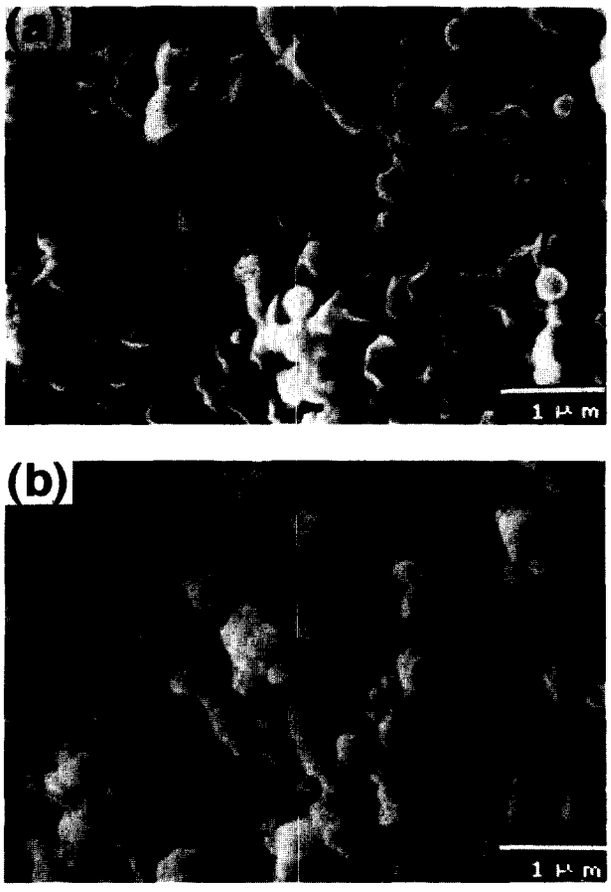

Fig. 8. SEM micrographs of fractured surface for specimens with (a) Y_2O_3 and (b) Yb_2O_3 addition quenched at 1400°C.

4 Discussion

4.1 Reaction process to form α'- and β'-sialons

From the results of the reaction sequence, change in phase composition and lattice parameters, possible reactions in the formation of α'- and β'-sialons are summarized in Table 1.

At the initial stage of liquid-phase sintering of sialon and Si_3N_4 ceramics, nitrides and oxide additives as well as impurities (oxides, metals and halogens) react to form a liquid, and subsequently, nitrogen glass and a partial crystalline phase appear at the grain boundaries. The phenomena are described by reaction (a). Here, the silica and alumina are the oxide impurities on the surface of raw Si_3N_4 and AlN particles.

α'-sialon is compatible with melilite. Furthermore, a α'-sialon with high solid solubility was observed at the initial stage. The reaction in precipitation of α'-sialon from a liquid are expressed as eqn (b). In the case of formation of α'-sialon with high solid solubility, reaction of α-Si_3N_4 with AlN and Ln_2O_3 should be considered, and eqn (c) is given. With respect to formation of α'-sialon at the initial stage, heterogeneous and homogeneous nucleation should be noted. The nucleation sites of α'-sialon formed at the initial stage were investigated by mean of TEM observation by Chatfield *et al.*[23] and Chen & Hwang.[24] Chatfield *et al.* reported that a core of unreacted α-Si_3N_4 raw material frequently remained in the α'-sialon particles, indicating that the unreacted α-Si_3N_4 raw material acts as nuclei for α'-sialon. Such a heterogeneous nucleation was also observed in sintering of β'-sialon.[23] On the other hand, the evidence of homogeneous nucleation of α'-sialon from a liquid matrix was not observed, but this event can not be discarded. The operation of heterogeneous and homogeneous nucleation of α'-sialon are thought to cause the change in solid solubility limits of the α'-sialon formed, and to greatly influence the thermal stability of α'-sialon, as will be mentioned later.

As the content of α'-sialon increases and lattice parameters decrease with raising the temperature, reaction (d) should be also considered. In the present work, it was not, however, possible to confirm the presence of α'-sialon with various solid solubilities, because the lattice parameters measured strike an average one of diverse solid solubilities.

Melilite disappeared due to precipitation of β'-sialon, and the chemical reaction in the formation of β'-sialon is expressed as eqn (e). It is also considered that precipitation of β'-sialon could proceed through reaction (f). Han *et al.*[25] investigated the phase transformation from α'-sialon to β'-sialon by liquid infiltration in the Y–Si–Al–N–O system, and they reported that during heating the glass matrix penetrated into the sintered α'-sialon specimen to induce the phase transformation of α'- into β'-sialon, and that no trace of α'-sialon existed in β'-sialon grains. Sugiyama *et al.*[26] investigated recently the thermal stability of α'-sialons with various solid solubility in mixed α'/β'-sialon. They reported that α'-sialon with a lattice parameter of the *c*-axis less than 5·65Å disappeared under heat-treatment at 1850°C for 50 h, and the amount of β'-sialon increased. On the other hand, the α'-sialon with a lattice parameter of the *c*-axis higher than 5·65Å remained after the heat-treatment, then its lattice parameters went up to nearly 5·66Å, and the amount of α'-sialon and β'-sialon decreased and increased, respectively. The former phenomena are anticipated to occur during precipitation of β'-sialon in the present work, since the increase in amount of α'-sialon is slowed by the formation of β'-sialon, and thereafter the amount of α'-sialon decreases slightly, as do, simultaneously, the lattice parameters. Consequently, reaction (f) is given.

4.2 Densification process

It is generally accepted that densification of Si_3N_4 ceramics with oxide additives and Si_3N_4 solid solu-

tions proceeds via liquid phase sintering, which consists of three stages: (I) particle rearrangement, (II) solution–precipitation and (III) coalescence of grains.[21,27] In the sintering process of sialon, several reactions to form the sialons, as described in the previous section, greatly influence the densification behavior. In the following section, the densification process of mixed α'/β'-sialon ceramics is discussed from the results of shrinkage, in connection with the reaction processes in the formation of sialons.

Shrinkage was initiated around 1200°C (Figs 1 and 2). The densification at the initial stage occurs by the rearrangement process, as the particles move to pack closer by capillary forces of the liquid.[27] It is well known that the temperature at which initial particle rearrangement occurs is related closely to the lowest eutectic temperature of oxides and impurities contained in the raw powders. Considering that SiO_2 and Al_2O_3 exist on the surface of Si_3N_4 and AlN particles, respectively, the eutectic liquid is the SiO_2–Al_2O_3–Ln_2O_3 system, whose minimum eutectic temperature is reported to be around 1450°C for Er_2O_3 addition.[28] Besides the oxide impurities, the liquidus temperature is reduced by the presence of metallic and halogen impurities. In this work, metallic impurities amounting to 350 ppm may be not high enough to reduce the liquidus temperature, but, on the other hand, a large amount of fluorine was present. In a previous work, Watari *et al.*[29] examined the effect of fluorine content (70, 440 and 670 ppm) in raw powders on the densification of Si_3N_4 ceramics with Y_2O_3 and Al_2O_3 addition by high-temperature dilatometry. They found that the temperature at which shrinkage starts decreased with increasing the fluorine content, and confirmed that shrinkage of Si_3N_4 powder with fluorine content of 670 ppm occurred at 1120°C. As the fluorine content in the raw powder used here is at the level of several hundred ppm, it must yield a reduction in the eutectic temperature.

In the case of sintering of Si_3N_4 ceramics, the influence of nitrogen ions on the liquid formation should also be considered. Hampshire & Jack[30] have pointed out that nitrogen as an additional component lowers the eutectic temperature by 100–200°C. In an experiment concerning nitrogen-glass preparation from the melting of a mixture of silica, alumina, lanthanide oxide and silicon nitride powders, the solubility of nitrogen ions in the liquid in the Si–Al–Y–O–N system is less than 15 at.%.[31] Wang *et al.*[32] have also mentioned that the solubility of nitrogen in Nd-sialon glass can reach 25 at.%, whereas in the Si–Al–Y–O–N system the highest solubility is only about 15 at.% and they also reported that the behavior of heavy rare-earth oxides is, in many aspects, similar to that of Y_2O_3. The solubility of nitrogen in a liquid is not, however, clarified in the sialon system. From the existence of impurities and nitrogen, it is, therefore, considered that reaction (a) of Table 1 occurs and that there is formation of a liquid phase around 1200°C, resulting in shrinkage due to initial particle rearrangement.

The next densification stage is due to a solution–precipitation process, which is accompanied by grain growth through the dissolution of small particles in the liquid and their reprecipitation on large particles.[27] In the fractured surface of the specimen sintered at 1400°C shown in Fig. 7 (b), the size and shape of particles are hardly distinguishable. After chemical etching for 15 min, roundish particles with a diameter of about 0·4 μm appeared, and they are different in size and shape from particles in the raw material shown in Fig. 7 (a). This microstructural change suggests that this temperature range corresponds to the solution–reprecipitation stage. Moreover, as shown in Fig. 7 (b) and (c), a large amount of glassy phase is formed, and it seems to have filled the interstice between particles. Such a phenomenon suggests that liquid flow is a significant densification mechanism at the solution–precipitation stage in sintering of Si_3N_4 ceramics.

At the solution–precipitation stage, reactions in formation of α'- and β'-sialons proceed through eqns (b), (c), (d), (e) and (f) of Table 1. The formation of α'-sialon yields reduction of the shrinkage rate at temperatures from 1510 to 1580°C for Er_2O_3 and at 1480 to 1580°C for Yb_2O_3 additions, because the ingredients in the liquid, i.e. lanthanide, aluminum and oxygen, are removed from it, causing the quantity and the viscosity of the liquid phase to decrease and to increase, respectively, interrupting then the dissolution of residual α-Si_3N_4 into the liquid. Furthermore, precipitation of melilite should be considered to hinder the densification process. As melilite formation consumes rare-earth cations, and it has a high melting point (~1900°C for yttrium-melilite[33] and >1700°C for samarium-melilite[34]), the amount of transient liquid is reduced over time. Consequently, the reduction of shrinkage rate at temperatures from 1480 to 1580°C is ascribed to formation of α'-sialon and melilite.

At temperatures higher than 1600°C, precipitation of β'-sialon and rapid increase of shrinkage rate occur concurrently, when Er_2O_3 and Yb_2O_3 were added. This increase of the shrinkage rate is associated with reactions in the formation of β'-sialon, indicated as eqns (e) and (f), which may induce the increase in liquid volume and the decrease in its viscosity, in contrast to the formation of α'-sialon, which causes the liquid volume to be

small and its viscosity high, and dissolution of residual Si_3N_4 into the liquid is difficult. As already mentioned, α'-sialon with low solid solubility is unstable thermodynamically during the sintering accompanied by formation of β'-sialon. Furthermore, disappearance of melilite occurs when β'-sialon precipitates. The acceleration of reactions (e) and (f) suggests that Ln_2O_3, which was accommodated into the α-Si_3N_4 structure or consumed by the formation of melilite, remains at the grain boundaries. In this case, it is postulated that an increase in the amount and a decrease in the viscosity of the liquid occur during precipitation of β'-sialon, and that the solution–precipitation process is, therefore, accelerated during the precipitation of β'-sialon. To date, the variations of volume and viscosity of liquid during the sintering of Si_3N_4 and sialon ceramics have not been measured in situ, and are the subject of absorbing interest when considering the liquid-phase sintering process of these materials. The authors have been considering that low-temperature specific heat and internal friction measurements can provide the information on the amount and viscosity of liquid during the heating.[35] The results concerning the character and quantity of liquid phase and grain boundary crystalline/glassy phase at various sintering temperature will be reported in the near future.

Figure 9 presents the isothermal shrinkage of compacts containing Yb_2O_3 addition with a heating rate of 10°C min^{-1}. When the heating rates of 30 and 50°C min^{-1} were used in preliminary experiments, the resultant amounts of α'-sialon and melilite formed at middle stage of sintering were small, indicating that a large amount of shrinkage took place. In this work, the heating rate was set at 10°C min^{-1} to clarify the densification process in rapid shrinkage at 1580 to 1700°C for Er_2O_3 and Yb_2O_3 additions. The kinetic parameter obtained takes values between 0·76 and 0·70, which are much larger than values predicted for the solution–precipitation process in the classical liquid-phase sintering model proposed by Kingery.[27] It is not possible here to clarify the sintering process through a mathematical analysis, and the densification can not be explained only by the solution–precipitation mechanism of the classical liquid-phase sintering model.

Since Kingery proposed a liquid-phase sintering model, a number of additional solution–precipitation mechanisms have been found, such as pore elimination due to cooperative flow of the particle–liquid mixture, Ostwald ripening with shape accommodation, and particle disintegration.[36] It is suggested that sintering of mixed α'/β'-sialon is a concurrent process involving these mechanisms. It

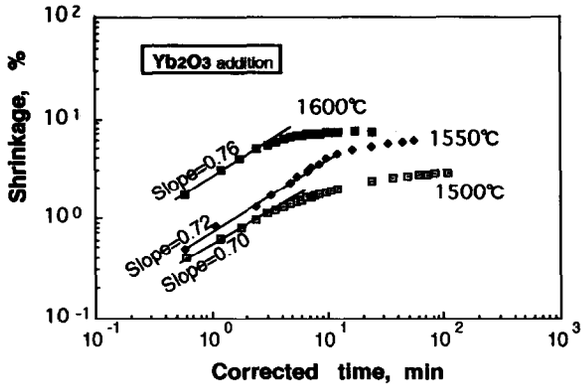

Fig. 9. Isothermal shrinkage of compacts with Yb_2O_3 addition.

is considered that the pore-elimination process due to cooperative flow of particle–liquid mixtures causes the rapid shrinkage observed at 1580 to 1700°C for Er_2O_3 and Yb_2O_3 additions and the kinetic parameters larger than any of the rate exponents predicted by Kingery' s model, since the rate of particle migration toward the interstices between particles is very fast. However, as shown in Fig. 1, the relative density at 1600°C was 80% for Er_2O_3 addition and 70% for Yb_2O_3 addition, which are much higher than a typical packing density of a monosized powder (64 vol.%). In this case, it can not be said that rapid shrinkage observed at 1580 to 1700°C for Er_2O_3 and Yb_2O_3 additions took place only by the particle migration process. It was expected from the results of Han *et al.* that in the present sintering, disintegration of α'-sialon grains occurs at temperatures higher than 1600°C, it then being easy for α'-sialon grains to migrate toward the interstice between particles, resulting in rapid shrinkage.

Besides these densification mechanisms, Ostwald ripening mechanism with shape accommodation is also anticipated to take place. In the present work, it was found that after sintering at 1850°C for 4 h, in the region containing the large grains, particles agglomerate, and large grains come into contact widely with other large ones (see Fig. 7 (h), the region surrounded with a white line). These microstructural features suggest that grain growth by Ostwald ripening occurs, grown grains contact with other ones, and subsequently the interstices between particles fill up by shape accommodation of grown grains. At the middle and final stages of sintering, this process is considered to help the densification further.

The densification process of mixed α'/β'-sialon ceramics has been discussed through the consideration of chemical reactions in formation of α'-sialon and β'-sialon and kinetical analysis of shrinkage. At the solution–precipitation stage, the formation of α'-sialon caused the retardation of densification, but during the formation of β'-

sialon, the densification proceeded rapidly. The densification at a latter stage relates to dissolution of α'-sialon formed at the early stage and of melilite into the liquid. From kinetical analysis, it was thought that dissolution of α'-sialon and melilite into the liquid and precipitation of β'-sialon induces the cooperative flow process of the particle–liquid mixture and particle disintegration process, besides the solution–precipitation process. Such an interpretation, however, may be too simplistic, and further work, such as identification of the disintegration of α'-sialon particles during heating, is necessary to understand the densification process exactly.

4.3 Effect of type of lanthanide oxide on densification and formation of sialon

The type of Ln_2O_3 added determines different sintering phenomena in mixed α'/β'-sialon ceramics and produces different amounts of α'- and β'-sialons. In Fig. 8, for Yb_2O_3 addition, the size and shape of particles can be identified, and the surface of particles is covered with a thin film of a material like a glassy-phase, which links neighboring particles. On the other hand, in the case of Y_2O_3 addition, the size and shape of particles are not well defined, because the particles seem to dissolve in the liquid. When Er_2O_3 is added, the microstructural feature (see Fig. (b)) is thought to be an intermediate microstructure between the corresponding to Yb_2O_3 and to Y_2O_3 addition. It is estimated from the microstructural features that in sintering at 1400°C for 15 min the amount and viscosity of the liquid for Y_2O_3 addition are, respectively, rather larger and lower than those for Er_2O_3 and Yb_2O_3 additions.

The resultant amounts of α'-sialon and melilite were different for each type of Ln_2O_3 addition. Recently, O'Reilly *et al.*[37] investigated the effect of diverse oxide additions on the sinterability of α'-sialon and on the resultant amounts of α'-sialon and melilite, and they summarized the correlation between the relative density and the amounts of these phases as functions of liquid volume and viscosity. Being the volume and viscosity of liquid different for diverse amounts of α'-sialon and melilite, the exact effect of the type of lanthanide oxide on densification can not be discussed. In this section, based on the reported data, the influence of the ionic radii of the lanthanide ion on the viscosity and amount of liquid is discussed without considering the effect of α'-sialon and melilite contents.

It has been reported that the eutectic temperature in the Si–O–N–M system, where M is a lanthanide, increases[38] and that the viscosity of glasses in the Si–Al–O–N–M system also increases[39] with decreasing ionic radius of the M ion. It is considered from these relations that at the initial stage of sintering, the liquidus temperature and viscosity of liquid formed decrease in the order of $Y_2O_3<Er_2O_3<Yb_2O_3$. Therefore, it is anticipated that for Y_2O_3 addition, solution–precipitation, liquid flow and cooperative flow of the particle–liquid mixture, as well as particle disintegration are accelerated, compared to Er_2O_3 and Yb_2O_3 additions.

As already mentioned, in the case of Er_2O_3 and Yb_2O_3 additions the formation of α'-sialon and melilite results in retardation of the shrinkage rate, while rapid shrinkage occurs when β'-sialon precipitates. However, as for Y_2O_3 addition, the retardation in shrinkage rate due to formation of α'-sialon and melilite was very slight. This is interpreted as dissolution of α'-sialon and melilite in the liquid and precipitation of β'-sialon occurring at an earlier stage.

5 Concluding remarks

The following conclusions can be drawn from this study:

(1) Possible reactions to form α'- and β'-sialons during the sintering of mixed α'/β' sialon ceramics were investigated from the results of reaction sequence, change in phase composition and lattice parameters. They were

$$SiO_2 + Al_2O_3 + Ln_2O_3 + Si_3N_4/AlN \rightarrow \text{Nitrogen glass} + \text{J-Phase } (Ln_4Si_2O_7N_2) \quad (a)$$

$$\text{J-Phase} + \text{Nitrogen glass} + Si_3N_4/AlN \rightarrow \alpha'\text{-Sialon}^H + \text{Melilite } (Si_3N_4 \cdot Ln_2O_3) + \text{Nitrogen glass} \quad (b)$$

$$Si_3N_4 + 9AlN \cdot Ln_2O_3 \rightarrow \alpha'\text{-Sialon}^H \quad (c)$$

$$Si_3N_4 + \alpha'\text{-Sialon}^H \rightarrow \alpha'\text{-Sialon}^L \quad (d)$$

$$Si_3N_4 + \text{Melilite} + \text{Nitrogen glass} \rightarrow \beta'\text{-Sialon} + \text{Nitrogen glass} \quad (e)$$

$$Si_3N_4 + \alpha'\text{-Sialon}^L + \text{Nitrogen glass} \rightarrow \beta'\text{-Sialon} + \text{Nitrogen glass} \quad (f)$$

where H and L indicate the α'-sialons with high and low solid solubility, respectively.

(2) As the formation of α'-sialon and melilite consumes the ingredients of the liquid, the densification is retarded over time. This phenomenon was clearly observed in sintering of mixed α'/β'-sialons containing Er_2O_3 and Yb_2O_3. On the other hand, during the formation of β'-sialon, densification was accelerated remarkably, and rapid shrinkage was observed. This is ascribed to the disso-

lution of α'-sialon with low solid solubility and melilite in the liquid and to precipitation of β'-sialon. It is, then, considered that volume and viscosity of liquid increase and decrease, respectively, resulting in acceleration of solution–precipitation, liquid flow, cooperative flow of the particle–liquid mixture, and particle disintegration.

(3) The type of lanthanide oxide strongly influences the sintering phenomena and phase composition. Densification at the initial and middle stages and reactions from α'-sialon and α-Si_3N_4 to β'-sialon accelerated in the order Y_2O_3 > Er_2O_3 > Yb_2O_3, because the liquidus temperature and viscosity of the liquid formed decrease in the order Y_2O_3 < Er_2O_3 < Yb_2O_3.

(4) The α'-sialon formed at the initial stage presented a high solid solubility in the α-structure, but thereafter lattice parameters decreased with elevating sintering temperatures. The x value in $Yx(Si, Al)_{12}(O,N)_{16}$ was 0·4 for the specimen obtained at 1500°C and 0·25 for the one at 1850°C. In the case of the β-structure, significant change in the lattice parameters were observed at temperatures between 1500 and 1600°C, and the value of z in the formula, $Si_{6-z}Al_zO_zN_{8-z}$ was 0·6 for the specimen sintered at temperatures higher than 1600°C. An influence of the type of the lanthanide oxide on lattice parameters was not apparent.

References

1. Lange, F. F., High-temperature strength behavior of hot-pressed Si_3N_4: evidence for subcritical crack growth. *J. Am. Ceram. Soc.*, **57** (1974) 84–7.
2. Becher, P. F., Microstructural design of toughened ceramics. *J. Am. Ceram. Soc.*, **74** (1991) 255–69.
3. Nagaoka, T., Watari, K., Yasuoka, M., Hirao, K. & Kanzaki, S., Interrelation between two and/or three-dimension grain morphology and fracture toughness of Si_3N_4 ceramics. *J. Ceram. Soc. Japan*, **100** (1992) 1256–60.
4. Kawashima, T., Okamoto, H., Yamamoto, H. & Kitamura, A., Grain size dependence of the fracture toughness of silicon nitride. *J. Ceram. Soc. Japan*, **99** (1991) 320–3.
5. Oyama, Y. & Kamigaito, O., Solid solubility of some oxides in Si_3N_4. *Japan. J. Appl. Phys.*, **10** (1972) 1637–42.
6. Jack, K. H. & Wilson, W. I., Ceramics based on the Si–Al–O–N and related system. *Nature*, **238** (1977) 28–9.
7. Hampshire, S., Park, K. H., Thompson, D. P. & Jack, K. H., α-sialon ceramics. *Nature*, **274** (1978) 880–2.
8. Huang, Z. K., Sun, W. Y. & Yan, D. S., Phase relations of the Si_3N_4–AlN–CaO system. *J. Mater. Sci. Lett.*, **4** (1985) 225–9.
9. Ishizawa, K., Ayuzawa, N., Shiratani, A., Takai, M., Uchida, N. & Mitomo, M., Some properties of α-sialon ceramics. In *Ceramic Materials and Components for Engines*, ed. W. Bunk & H. Hausner. German Ceramic Society, Bad Honnef., Germany, 1986, pp. 511–18.
10. Nagel, A., Greil, P. & Petzow, G., Reaction of sintering of yttrium containing α-silicon nitride solid solution. *Revue de Chemie Minerale*, **22** (1985) 437–47.
11. Slasor, S. & Thompson,. D. P., Preparation and characterization of α'-sialons. In *Non-Oxide Technical and Engineering Ceramics*, ed. S. Hampshire. Elsevier, London, 1986, pp. 223–30.
12. Mitomo, M., Hasegawa, Y., Bando, Y., Watanabe, A. & Suzuki, H., The strength of hot-pressed β-sialon. *Yogyo-Kyokai-Shi*, **88** (1980) 78–84.
13. Umebayashi, S., Kishi, K., Tani, E. & Kobayashi, K., The strength of hot-pressed β-sialons with Z = 1 in $Si_{6-z}Al_zO_zN_{8-z}$. *Yogyo-Kyokai-Shi*, **92** (1984) 35–51.
14. Tanaka, I., Pezzotti, G., Miyamoto, Y. & Okamoto, T., Fracture toughness of Si_3N_4 and its Si_3N_4 whisker composite without sintering aids. *J. Mater. Sci.*, **26** (1991) 208–10.
15. Ekstrom, T. & Nygren, M., Sialon ceramics. *J. Am. Ceram. Soc.*, **72** (1992) 259–76.
16. Ukyo, Y. & Wada, S., High strength Si_3N_4 ceramics. *J. Ceram. Soc. Japan*, **97** (1989) 872–4.
17. Cao, G. Z., Metselaar, R. & Ziegler, G., Relations between composition and microstructure of sialons. *J. Eur. Ceram. Soc.*, **11** (1992) 115–22.
18. Jack, K. H., Sialon ceramics: retrospect and prospect. In *Silicon Nitride Ceramics—Scientific and Technological Advances, Materials Research Society Proceedings*, Vol. 287, ed. I.-W. Chen, P. F. Becher, M. Mitomo, G. Petzow & T.-S. Yen. Materials Research Society, Pittsburgh, 1993, pp. 15–28.
19. Mandal, H., Thompson, D. P. & Ekstrom, T., Reversible α–β sialon transformation in heat-treated sialon ceramics. *J. Eur. Ceram. Soc.*, **12** (1993) 421–9.
20. Ekstrom, T., Ingelstrom, N., Brage, R., Hatcher, M. & Johansson, T., α–β Sialon ceramics made from different silicon nitride powders. *J. Am. Ceram. Soc.*, **71** (1988) 1164–70.
21. Abe, O., Sintering process of Y_2O_3-added Si_3N_4. *J. Mater. Sci.*, **25** (1990) 3641–8.
22. Ukyo, Y. & Wada, S., Formation and stability of Y-α'-sialon co-existing with β'-sialon. In *Euro-Ceramics*, Vol. 1., ed. G. de With. A. Terpstra & R. Metselaar. Elsevier Science, London, 1989, pp. 566–72.
23. Chatfield, C., Ekstrom, T. & Nikus, M., Microstructural investigation of alpha–beta yttrium sialon materials. *J. Mater. Sci.*, **21** (1986) 2297–307.
24. Chen, I.-W. & Hwang, S.-L., Superplastic sialon—a bird's eye view of silicon nitride ceramics. In *Silicon Nitride Ceramics—Scientific and Technological Advances—Materials Research Society Proceedings*, Vol. 287, ed. I.-W. Chen, P. F. Becher, M. Mitomo, G. Petzow & T.-S. Yen. Materials Research Society, Pittsburgh, 1993, pp. 209–22.
25. Han, S. M., Kang, S.-J. & Lee, Y.-T., Phase transformation from α' to β'-sialon by liquid infiltration in Y–Si–Al–O–N system. *J. Eur. Ceram. Soc.*, **12** (1993) 431–4.
26. Sugiyama, N., Ukyo, Y. & Wada, S., Thermal stability of phases in Si_3N_4 (–SiO_4)–AlN–Y_2O_3 system. *J. Ceram. Soc. Japan*, **102** (1994) 145–8.
27. Kingery, W. D., Densification during sintering in the presence of a liquid phase: I. *J. Appl. Phys.*, **30** (1969) 301-6.
28. Murakami, Y. & Yamamoto, H., Phase equilibria and properties of glasses in the Al_2O_3–Yb_2O_3–SiO_2 system. *J. Ceram. Soc. Japan*, **101** (1993) 1101–6.
29. Watari, K., Kanzaki, S., Asayama, M., Tsuge, A., Isozaki, K. & Hirotsuru, H., Influence of halogen impurities in raw powder on sinterability of Si_3N_4 ceramics, In *Proceedings of Annual Meeting of the Ceramics Society of Japan*. Ceramics Society of Japan, Tokyo, 1993, p. 610.
30. Hampshire, S. & Jack, K. H., The kinetics of densification and phase transformation of nitrogen ceramics. *Proc. Brit. Ceram. Soc.*, **31** (1980) 37–49.

31. Loehman, R. E., Preparation and properties of yttrium–silicon–aluminium oxygen nitride glasses. *J. Am. Ceram. Soc.*, **62** (1979) 491–4.
32. Wang, P. L., Sun, W. Y. & Yen, T. S., Formation and densification of R–α'-sialons (R = Nd, Sm, Gd Dy, Er and Yb). In *Silicon Nitride Ceramics—Scientific and Technological Advances—Materials Research Society Proceedings*, Vol. 287, ed. I.-W. Chen, P. F. Becher, M. Mitomo, G. Petzow & T.-S. Yen. Materials Research Society, Pittsburgh, 1993, pp. 387–92.
33. Jack, K. H., Silicon nitride, sialons, and related ceramics. In *Ceramics and Civilization*, Vol. III, *High-Technology Ceramics*. American Ceramics Society, Columbus, OH, 1986, pp. 259–88.
34. Cheng, Y.-B. & Thompson, D. P., Aluminium-containing nitrogen melilite phases. *J. Am. Ceram. Soc.*, **77** (1994) 143–8.
35. Watari, K., Sakaguchi, S., Kanzaki, S., Hamasaki, T. & Ishizaki, K., Quantity and character of grain boundary phase in mixed α'/β'-sialon ceramics. *J. Mater. Res.*, **9** (1994) 2741–4.
36. Petzow, G. & Kaysser, W. A., Basic mechanisms of liquid-phase sintering. In *Sintering Key Papers*, ed. S. Somiya & Y. Moriyoshi. Elsevier Applied Science, London and New York, 1990, pp. 595–614.
37. O'Reilly, K. P., Redington, M., Hampshire, S. & Leigh, M., Parameters affecting pressureless sintering of α'-sialons with lanthanide modifying cations. In *Silicon Nitride Ceramics—Scientific and Technology Advances—Materials Research Society Proceedings*, Vol. 287, ed. I.-W. Chen, P. F. Becher, M. Mitomo, G. Petzow & T.-S. Yen. Materials Research Society, Pittsburgh, 1993, pp. 393–9.
38. Gazza, G. E., *Progress in Nitrogen Ceramics (NATO ASI Series)*, ed. F. L. Riley. Martinus Nijhoff, The Hague, Netherlands, 1983, p. 273.
39. Drew, R. A. (ed.), *Nitrogen Glass*. Research Reports in Materials Science, The Parthenon Press, Castertonhall, Lancashirela, UK, 1986, Fig. VII. 9.

Appendix

As has been pointed out by many investigators, characteristics of raw Si_3N_4 powders such as the amount, type and distribution of impurities, grain size and particle distribution influences greatly the sintering behavior, sinterability, microstructural development and mechanical properties of sintered materials, as well as the amount and composition of the grain boundary crystalline/glassy phase. Experimental results of the shrinkage rate obtained by high-temperature dilatometry measurements provide some useful information to evaluate the relationships between the characteristics of raw Si_3N_4 powders and densification behavior. Figure A1 shows the temperature dependence of shrinkage rate of compacts, whereas the characteristics of raw Si_3N_4 powders are shown in Table A1. As can be observed, sintering behavior and sinterability are greatly influenced by the type of raw powder. The temporary retardation of shrinkage rate due to formation of α'-sialon and melilite can be seen at temperatures between 1500 and 1600°C in Fig. A1, irrespective of the characteristics of raw powders; however, the densities of specimens obtained from the powders C, D and E are very much lower than the densities of those from the powders A and B. The significant parameters affecting the densification are not clarified at present.

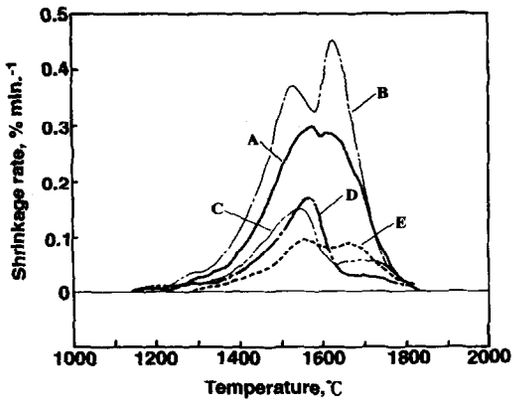

Fig. A1. Influence of powder characteristics on shrinkage rate of Si_3N_4 compacts with 1·69 mol% AlN and 15·21 mol% Y_2O_3. The characteristics of the powders used are shown in Table A1. After thermal shrinkage measurements at 1850°C for 15 min, the relative density was 85·5% for powder A, 89·2% for powder B, 63·9% for powder C, 65·2% for powder D, and 64·8% for powder E.

Table A1. Representative properties of raw Si_3N_4 powder

Raw powder	*Specific surface area* ($m^2\ g^{-1}$)	*Oxygen content* (*wt%*)	*Carbon content* (*wt%*)	*α-Phase content* (%)
A	11·3	1·30	0·11	94·0
B	10·5	1·20	0·14	90·1
C	12·4	1·00	0·04	90·2
D	11·1	0·8	0·05	90·4
E	9·9	1·2	0·02	98·0